

Article

ProDOT-Based Polymers: From Energy Storage to Smart Window Applications

Adriana-Petronela Chiriac, Catalin-Paul Constantin  and Mariana-Dana Damaceanu *

Electroactive Polymers and Plasmachemistry Laboratory, “Petru Poni” Institute of Macromolecular Chemistry, Aleea Grigore Ghica Voda 41A, 700487 Iasi, Romania

* Correspondence: damaceanu@icmpp.ro

Abstract: Nowadays, electroactive materials based on conjugated polymers for energy storage and electrochromic window applications attract large interest due to their low cost, accessible synthetic procedures, and interesting electrochemical properties. Herein, we report on the performance of two propylenedioxythiophene (ProDOT)-based polymers having varying length and functionality side chains, which were explored to assess their potential for these applications. The polymers were obtained by oxidative chemical polymerization and processed from organic solvents into thin coatings with different molecular assemblies. Preliminary studies on their chemical structure and optical and electrochemical characteristics were performed to evidence how these are influenced by the side chain substituent nature. When tested as electrode material in the three-electrode cell configuration, the synthesized ProDOT-based polymers provided the highest specific areal capacitance of 1.059 mF/cm² at a scan rate of 10 mV/s and 0.538 mF/cm² at 0.01 mA/cm² in cyclic voltammetry and galvanostatic charge–discharge measurements, respectively. One of the polymers showed electrochromic response, with ultrafast color change from deep purple to highly transmissive green/blue. A coloration efficiency of 123 cm²/C and a maximum CE decay of 9.9% after 100 cycles was achieved for this material, which is also able to efficiently store electrical charge, thus demonstrating potential for use in energy storage smart window applications where the energy level can be estimated by simple visual observation.

Keywords: propylenedioxythiophene; conjugated polymers; side chain functionality; energy storage; electrochromism



Citation: Chiriac, A.-P.; Constantin, C.-P.; Damaceanu, M.-D. ProDOT-Based Polymers: From Energy Storage to Smart Window Applications. *Energies* **2023**, *16*, 3999. <https://doi.org/10.3390/en16103999>

Academic Editor: Daniel T. Hallinan, Jr.

Received: 4 April 2023
Revised: 4 May 2023
Accepted: 6 May 2023
Published: 9 May 2023



Copyright: © 2023 by the authors. Licensee MDPI, Basel, Switzerland. This article is an open access article distributed under the terms and conditions of the Creative Commons Attribution (CC BY) license (<https://creativecommons.org/licenses/by/4.0/>).

1. Introduction

Conducting polymers, as one of the most important classes of conjugated polymers, are often explored for use in applications nowadays, including electrochromic devices, sensors, actuators, and smart windows [1,2], but also for energy storage in supercapacitors, batteries, fuel cells, or for energy harvesting, in solar cells [3,4]. The most attractive polymers include polypyrroles, polyphenylenes, polyfurans, polyanilines, polyacetylene, and polythiophenes [5,6], which can be easily processed by simple solution-based methods such as spin-coating, drop-casting, spraying, or dip-coating, but also by advanced patterning methods like inkjet printing [7]. Among them, polythiophenes emerged as well-known conducting polymers due to their remarkable stability towards oxygen and moisture, and unique optoelectronic properties that endowed them with a great potential for use as advanced materials in the development of organic thin film transistors, light emitting diodes, solar cells, supercapacitors, sensors, etc. [8,9].

3,4-Alkylenedioxythiophene-based polymers are particular derivatives of polythiophenes which display reduced oxidation potential, favorable electrical conductivity, good stability in the oxidized state, and high chemical stability, especially those based on 3,4-propylenedioxythiophene (ProDOT) [10]. These can be directly synthesized by oxidative chemical polymerization or electropolymerization, leading to materials with appealing

physical and chemical properties [1,11]. However, they are rarely obtained by chemical oxidative polymerization due to the low solubility and processability of the resulted polymers in accessible solvents. Instead, electrochemical polymerization is preferred due to several advantages, such as short reaction time, reproducibility, and the ability to provide coatings directly on the electrodes, whose thickness and morphology can be precisely controlled [12–14]. One important characteristic of ProDOT-based polymers is their ability to undergo a reversible color change following electron transfer upon application of an electric potential, a phenomenon known as electrochromism [15,16]. These polymers render excellent electrochromic performance due to their favorable redox properties, including enhanced optical contrast and fast switching kinetics in organic and aqueous electrolytes, and the capability of switching between colored and bleached states during oxidation [17]. For instance, a ProDOT-based polymer functionalized with oligoether units at the 2-position of the propylene bridge, namely ProDOT(OE)-DMP reported by Savagian et al. [18], showed high redox activity in both aqueous and non-aqueous electrolytes, oxidation onsets lower than 0 V vs. Ag/AgCl, high contrast ($\Delta T > 70\%$), fast switching (1 s) in NaCl_{aq} , and charge-storage capacity over 80 F/g when used as an active material in organic electrochemical transistors. A comparison between the redox and electrochromic properties of related ProDOT-based polymers bearing diverse functionalities, such as ProDOT-(OEtHx)₂, ProDOT-Am(EtHx), and ProDOT-Am(Butyl)₂, highlighted that ether functionalized polymers show only minor electrochemical activity at very high voltages, while the amide functionalized polymers showed lower oxidation onsets and a high and stable electrochromic contrast upon repeated color switching between their colored and bleached states [17].

On the other hand, the electrochemical properties of ProDOT-based polymers make them suitable for electrical charge storage applications, and thus these polymers can be used in supercapacitors, which are characterized by high power density, high capacitance, long-term stability, long cycle life, and fast charge/discharge capability [19,20]. Niu et al. [21] explored the capacitance performance of a symmetrical supercapacitor based on poly((3,4-dihydro-2H-thieno [3,4-b][1,4]dioxepin-3-yl)methanol) (PProDTM) nanowire in aqueous and organic electrolytes, when a specific capacitance of 89.2 F/g was obtained at current density of 1.0 A/g in 0.1 M H₂SO₄ and a slightly higher value of 99.6 F/g, in 0.1 M Bu₄NBF₄. Moreover, Sarac et al. [22] investigated the capacitance behavior of poly(2,2-dimethyl-3,4-propylenedioxythiophene)—PProDOT(Me)₂ obtained by electropolymerization on carbon fiber, and they found a capacitance of 12.05 mF/cm². Later, this electroactive polymer was studied for its electrochromic properties [2] when a color contrast of 60% at a low applied potential (1.2 V) was obtained. The switching speed for coloring and bleaching was almost 0.7 s in the potential window between +1.5 and −1.5 V. Several other polymers derived from ProDOT functionalized with different groups e.g., PDBProDOT (a 2,3-dibenzyl derivative), PProDOT-Et₂ (a 2,2-diethyl derivative), and PProDOT-EtO-BZA (an oligoether substituted with an aromatic carboxylic ester group derivative) were compared with regard to their capacitive behavior [20]. It was found that PProDOT-EtO-BZA revealed pseudocapacitive behavior, with specific and low-frequency capacitance of 20.8 mF/cm² and 8.5 mF/cm², respectively. These results were almost two times higher than those of the related derivatives, proving the capability of PProDOT-EtO-BZA films to be used as electrode material in supercapacitors. It should be noted that all these ProDOT polymers were obtained by electrochemical polymerization.

Since both the electrochromic and capacitive mechanisms share redox reactions, those two functions can be provided by a single electrode material in a unique electrochemical cell, which can be applied to develop energy storage smart windows (ESSWs) [23]. Only limited polymers were exploited for this purpose, among which polyaniline is the most widely used because of its various benefits, such as high energy storage capability, high redox reversibility, multiple stable doping states, and inexpensive cost [24]. Although polythiophene and derivatives have also demonstrated great potential for use in ESSWs, little has been done to exploit these materials as electrochromic and capacitive electrodes,

C–C_{ProDOT} stretches), 1184 cm⁻¹ (C–O–C stretch), 1019 cm⁻¹ (alkylenedioxy group stretch), and 778 cm⁻¹ (C–S_{Th} stretch).

ProDOT-ester:

¹H-NMR (CDCl₃), δ (ppm): 7.99–7.96 (2H, dd, H-17, H-18), 6.93–6.91 (2H, dd, H-15, H-16), 6.46 (2H, s, H-1, H-4), 4.36–4.31 (2H, quartet, H-21), 4.18–4.15 (2H, t, H-13), 4.02–3.99 (2H, d, H-5, H-6), 3.88–3.86 (2H, t, H-12), 3.73–3.64 (6H, m, H-5, H-6, H-10, H-11), 3.54 (2H, s, H-9), 1.39–1.36 (3H, t, H-22), 0.97 (3H, s, H-8).

¹³C-NMR (CDCl₃), δ (ppm): 166.29 (C-9), 162.44 (C-14), 149.82 (C-23), 131.44 (C-17, C-18), 123.01 (C-19), 114.08 (C-15, C-16), 105.53 (C-1, C-4), 77.33–76.63 (C-5, C-6), 73.71 (C-9), 71.14–70.65 (C-10, C-11), 69.50 (C-12), 67.55 (C-13), 60.56 (C-21), 43.35 (C-7), 17.27 (C-8), 14.32 (C-22).

FTIR (ATR): 3108 cm⁻¹ (C–H_{Ar}, C–H_{Th} stretch), 2963–2873 cm⁻¹ (C–H_{aliphatic} stretch), 1707 cm⁻¹ (C=O_{ester} stretch), 1607 cm⁻¹, 1510 cm⁻¹, 1484 cm⁻¹, 1449 cm⁻¹, 1366 cm⁻¹ (C=C and C–C stretches in Th and Ph), 1274 cm⁻¹, 1251 cm⁻¹ (C–O stretch in the oligo-oxyethylene group), 1057 cm⁻¹, 1021 cm⁻¹ (alkylenedioxy group of ProDOT stretch), 848 cm⁻¹ (C–S_{Th} stretch).

2.3. Synthesis of Polymers

Two ProDOT-based polymers, denoted as PProDOT-OH and P(ProDOT-ester), were prepared by the oxidative chemical polymerization reaction of ProDOT-OH and ProDOT-ester, respectively, in chloroform (CHCl₃), in the presence of ferric chloride (FeCl₃) as an oxidative reagent, followed by a dedoping process using ammonium hydroxide (NH₄OH). To illustrate the general synthetic procedure, the detailed pathway for the preparation of PProDOT-OH is further provided. In a Schlenk tube (V = 25 mL), 0.06 g (0.299 mmol) ProDOT-OH dissolved in 10 mL CHCl₃ was placed, and then 0.0971 g (0.598 mmol) FeCl₃ was added under stirring and nitrogen flow. The obtained dark blue suspension was maintained under stirring at room temperature for 28 h. Then, 1 mL of concentrated aqueous ammonium solution was introduced in the system to dedop the polymer. The stirring was continued for another 40 h when the suspension changed from black-blue to black-reddish. Finally, the reaction mixture was poured into MeOH to precipitate the polymer. After filtration, a brown solid was obtained, which was washed several times with hot MeOH and dried to get a dark brown polymer powder. P(ProDOT-ester) was synthesized by a similar procedure, being obtained as a dark violet solid.

PProDOT-OH:

¹H-NMR (CDCl₃), δ (ppm): 4.22–4.10 (3H, m), 3.94 (1H, t, OH), 3.71–3.68 (1H, dd), 3.62–3.58 (1H, dd), 0.85 (3H, s).

FTIR (ATR): 3312 cm⁻¹ (–OH), 2976–2879 cm⁻¹ (C–H_{aliphatic} stretch), 1642 cm⁻¹, 1502–1473 cm⁻¹ and 1359–1340 cm⁻¹ (C=C and C–C of ProDOT stretches), 1175 cm⁻¹ (C–O–C stretch), 1039 cm⁻¹ (alkylenedioxy group stretch), and 862 cm⁻¹ (C–S_{Th} stretch).

P(ProDOT-ester):

¹H-NMR (CDCl₃), δ (ppm): 7.94 (2H, s), 6.89 (2H, s), 4.31–4.15 (m, 6H), 3.89–3.71 (m, 10H), 1.34 (m, 3H), 1.06 (s, 3H).

FTIR (ATR): 3075 cm⁻¹ (C–H_{Ar}), 2978–2867 cm⁻¹ (C–H_{aliphatic} stretch), 1704 cm⁻¹ (C=O_{ester} stretch), 1605 cm⁻¹, 1509 cm⁻¹, 1470 cm⁻¹, 1434 cm⁻¹, 1362 cm⁻¹ (C=C and C–C stretches in Th and Ph), 1275 cm⁻¹, 1250 cm⁻¹ (C–O stretch in the oligo-oxyethylene group), 1043 cm⁻¹, 1022 cm⁻¹ (alkylenedioxy group of ProDOT stretch), 847 cm⁻¹ (C–S_{Th} stretch).

2.4. Preparation of Polymer Films

Very diluted polymer solutions in different solvents (DCM, DMF, or NMP) of 0.5% concentration were dropped onto glass, quartz, and ITO-coated glass plates to obtain polymer thin coatings. Prior to this, all solutions were filtered through a 0.45 μm filter membrane. The residual solvent was removed following a gradual heating process up to the boiling temperature of each solvent and maintained at this temperature for 1–2 h. The obtained

coatings were further used to explore the optical, electrochemical, spectroelectrochemical, and capacitive characteristics of the polymers.

2.5. Measurements

Structural characterization of the monomers and polymers was carried out by Nuclear Magnetic Resonance spectroscopy—NMR (^1H - and ^{13}C -NMR) and Fourier-transform infrared spectroscopy (FTIR). The NMR spectra were recorded on a Bruker Avance III 400 spectrometer using deuterated acetone or deuterated chloroform. ^1H and ^{13}C chemical shifts are provided in δ units (ppm) relative to the residual peak of the solvent (ref. ^1H , $(\text{CD}_3)_2\text{CO}$: 2.05 ppm, ^{13}C , $(\text{CD}_3)_2\text{CO}$: 29.84 ppm; ^1H , CDCl_3 : 7.26 ppm, ^{13}C , CDCl_3 : 77.16 ppm). The FTIR spectra were registered on an FT-IR Bruker Vertex 70 Spectrophotometer in the reflexion mode, by ATR technique.

The average molecular weights were evaluated by gel permeation chromatography (GPC) using a ParSEC Chromatography Ver. 5.67 (Brookhaven Instruments Corp., Holtsville, NY, USA) equipment containing refraction and UV detectors and PL Mixed C Column. The measurements were carried out in DMF as the solvent, with polymer solutions prepared at a concentration of 1%, after filtration. Standards of polystyrene of known molecular weight were used for calibration.

The morphology of the polymer coatings was evaluated by atomic force microscopy (AFM) using a Scanning Probe Microscopy Solver PRO-M, NT-MDT equipment from Russia, in semi-contact mode, semi-contact topography technique.

The UV-vis spectra were recorded on a Shimadzu UV-1280 spectrophotometer, whereas the fluorescence (FL) spectra were obtained with a Shimadzu RF-6000 spectrofluorophotometer. Both very diluted solution samples (approx. 10^{-5} M) in different solvents like DCM, NMP, DMF, and coatings on quartz plates were used for these measurements.

The electrochemical characteristics were studied on a Potentiostat—Galvanostat (PG581, Uniscan Instruments, Buxton, United Kingdom) by using cyclic voltammetry (CV) and chronopotentiometry to register the galvanostatic charge–discharge curves (GCD). The three-electrode electrochemical cell was fitted with ITO-coated polymer as the working electrode, platinum wire as the auxiliary electrode, and Ag/AgCl as the reference electrode. The capacitive behavior was screened in different electrolyte systems (0.1 M TBAP/ACN, 0.1 M TBAF/can, and 0.1 M LiClO_4 /ACN). All measurements were realized in an ambient atmosphere, at a scan rate of $50 \text{ mV} \times \text{s}^{-1}$.

Spectroelectrochemical curves were obtained on a Potentiostat—Galvanostat (Autolab PGSTAT204) coupled with a UV-vis spectrophotometer. Lithium perchlorate (10^{-2} M LiClO_4)/ACN) was employed as the electrolyte in a UV cuvette equipped with ITO-coated polymer as the working electrode, platinum wire as the auxiliary electrode, and Ag wire as the reference electrode.

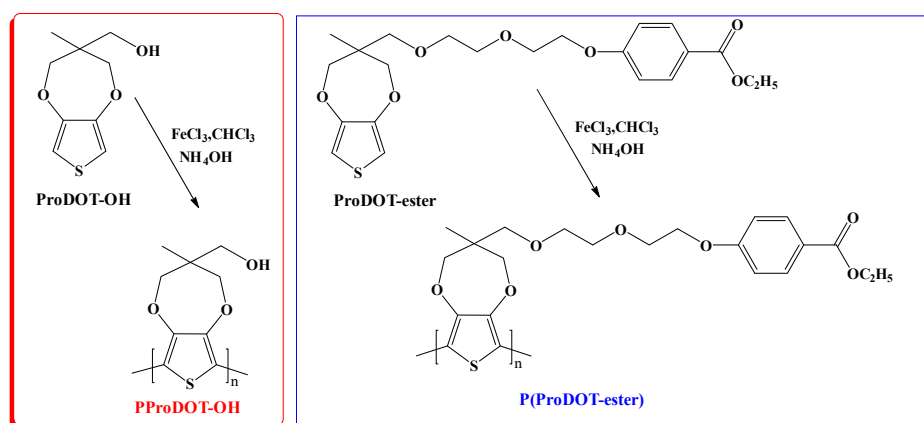
Electrical impedance spectroscopy (EIS) measurements were recorded on the same Autolab Potentiostat—Galvanostat in the frequency range of 100 mHz–1 MHz. The experiments were performed in the same electrolyte systems used for CV studies at 0 V.

3. Results and Discussions

3.1. Structural Characterization

To be used in ESSW applications, the electrode material must integrate both energy storage and electrochromic functions. Since ProDOT-based polymers have separately demonstrated both excellent energy storage capacity and electrochromic behavior [16,22], these were selected as active materials for ESSWs. The nature of the functional side group is expected to tune the envisaged characteristics of ProDOT-based polymers, and therefore an exhaustive study was performed to assess the influence of the side chain structure on the overall performance. To this aim, two ProDOT-based polymers functionalized with CH_2OH or aromatic ester substituted oligo-oxethylene side chains, namely PProDOT-OH and P(ProDOT-ester), respectively, were synthesized by oxidative chemical polymerization, according to Scheme 1. Both polymers demonstrated limited solubility in THF, CHCl_3 ,

and DCM, and moderate solubility in DMF, DMAc, and NMP. As a consequence, only the soluble fractions in these solvents were used for further investigations. However, P(ProDOT-ester) displayed a better solubility, especially in high polar solvents, compared to PProDOT-OH, which strongly aggregated, mostly due to the intermolecular H-bonds developed by the OH groups of the side chains. The good solubility of P(ProDOT-ester) enabled molecular weight evaluation by gel permeation chromatography (GPC) versus polystyrene standards for the DMF-soluble fractions. Thus, the weight average molecular weight (M_w) was 81,000 Dalton, the number average molecular weight (M_n) was 49,000 Dalton, and the polydispersity index (M_w/M_n) was 1.66. These values are higher than those obtained for other ester-derivatives of poly(propylenedioxythiophene) [26,27], whereas the polydispersity (below 2) was similar. The highest values obtained for P(ProDOT-ester) in DMF can be due to more planar conformation and more extensive conjugated form of the polymer chains in DMF compared to CHCl_3 or THF that were used by other authors for GPC measurements when the macromolecules are in a more twisted form. Unfortunately, the solubility of PProDOT-OH in DMF was too low, and any attempt to accurately evaluate the molecular weights failed.



Scheme 1. The synthetic pathways to polymers PProDOT-OH and P(ProDOT-ester).

The structural identification of ProDOT-based polymers was accomplished by FTIR and NMR spectroscopies in comparison with those of the starting monomers. The $^1\text{H-NMR}$ spectra of the polymers (Figure 2) highlighted broad signals and the absence of the 1,4-thienyl protons, which were observed for the monomers at 6.57 ppm (ProDOT-OH) and 6.46 ppm (ProDOT-ester), demonstrating the successful incorporation of ProDOT unit into polymer structures.

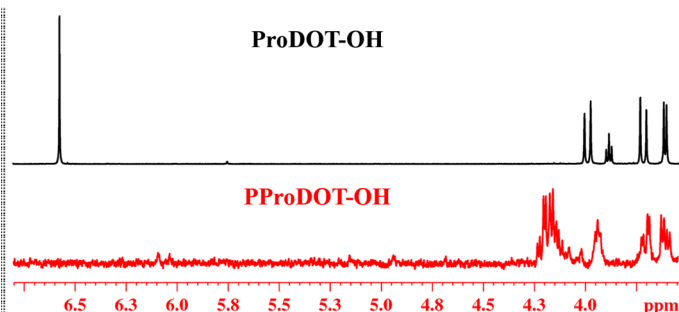


Figure 2. Comparative $^1\text{H-NMR}$ spectra of ProDOT-OH and PProDOT-OH.

The comparison between FTIR spectra of the synthesized ProDOT-based monomers and polymers is illustratively presented in Figure 3 for the CH_2OH functional group anchored on ProDOT. Generally, all characteristic bands were identified in polymers at slightly shifted values relative to those of the corresponding monomer. For instance, the

strong absorption band at 3300 cm^{-1} , characteristic of the OH group of the monomer, was identified at 3312 cm^{-1} in the case of polymer, while the intense sharp band at 1707 cm^{-1} associated with the C=O stretching of the ester functional group registered an insignificant shift, being observed at 1704 cm^{-1} . The most prominent feature noticed in the case of polymers was the absence of the thienyl C-H stretching vibration identified at about 3100 cm^{-1} for the monomers.

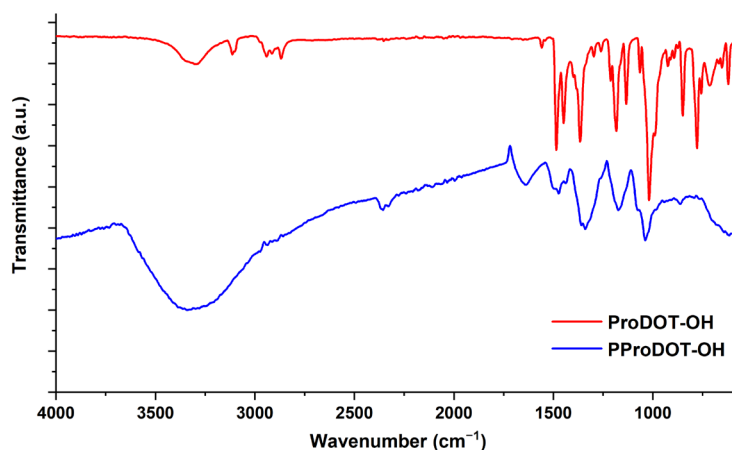


Figure 3. Comparative FTIR spectra of ProDOT-OH and PProDOT-OH.

3.2. Optical Properties

The optical properties of ProDOT-based monomers and polymers were comparatively investigated by UV-Vis and fluorescence (FL) spectroscopies. First, the spectra were registered for the monomers to survey their electronic transitions and the influence of the substituent nature attached to the ProDOT unit on these transitions. Figure 4 shows the UV-vis absorption and fluorescence spectra of the two monomers recorded in the dichloromethane (DCM) solution.

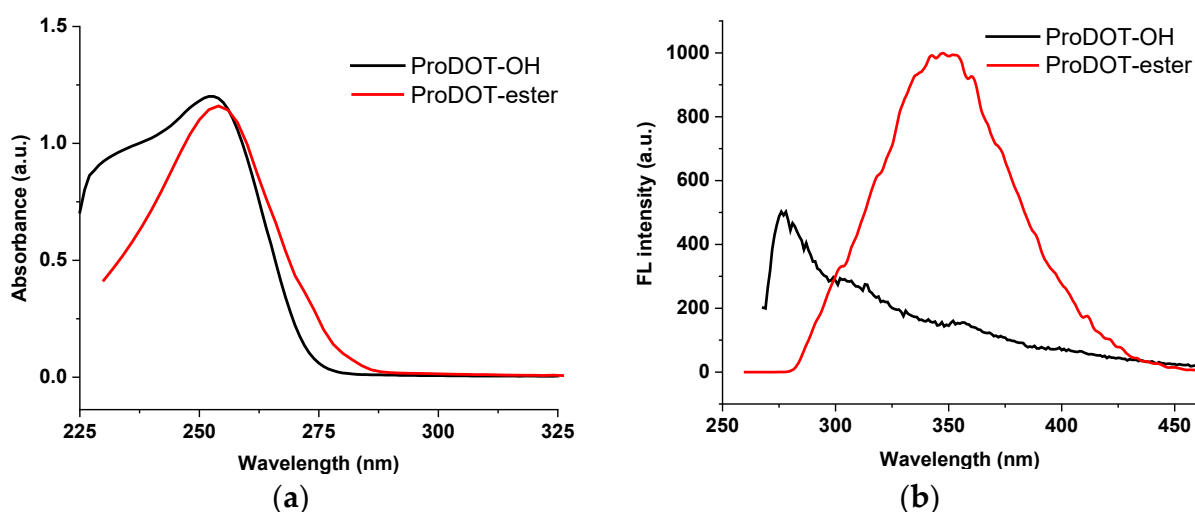


Figure 4. UV-vis absorption (a) and fluorescence (b) spectra of the ProDOT-based monomers.

As seen in Figure 4, all monomers display a single well-resolved absorption band of high intensity, with the maximum at 252 and 254 nm for ProDOT-OH and ProDOT-ester, respectively, which can be attributed to the $\pi\text{-}\pi^*$ and $n\text{-}\pi^*$ transitions occurring in the ProDOT unit. In the case of the monomer functionalized with the ester group, these transitions overlapped with the $\pi\text{-}\pi^*$ ones of the benzene ring, which are observed in the form of a shoulder-like peak at 273 nm. A slight shift of the absorption maximum was noticed in

dependence with the attached substituent, which proves that the electronic transitions of the ProDOT unit are influenced by the chemical structure of the substituent. This induces different conformation and planarity of the ProDOT monomer, with direct impact on the electronic transitions. Excitation with UV light corresponding to the absorption maximum wavelength led to fluorescence spectra centered at different wavelengths, also depending on the substituent. Thus, in the case of ProDOT-ester, a strong emission band centered at 349 nm was obtained, while ProDOT-OH showed a broad and weak fluorescence band with a maximum at 277 nm and two shoulders centered at about 307 and 357 nm. The strong fluorescence of ProDOT-ester most likely originates from the oligo-oxyethylene and ester-containing group anchored on ProDOT.

Figure 5 shows the UV-vis absorption and fluorescence spectra of both polymers obtained by oxidative polymerization (P(ProDOT-ester) in DMF, PProDOT-OH in NMP). The UV-Vis absorption spectra of P(ProDOT-ester) highlighted absorptions at lower energies with respect to the monomer, proving the existence of an extended polymer chain conjugation. The spectral pattern consisted of one absorption band with three maxima (542 nm, 575 nm, 625 nm) that are associated with the π - π^* transitions occurring in the conjugated polymer molecules having different conformations (conjugation lengths). A more planar conformation generally leads to a more extended conjugation and, consequently, to an absorption of visible light at higher wavelength. A different optical response was noticed for PProDOT-OH that displayed a single intense absorption band centered at lower wavelength (494 nm). This suggests a less extensive conjugation than in the case of the ester-functionalized polymer, and a better homogeneity of the conformation and conjugation length. In addition to the main absorption band, this polymer also showed a very weak absorption with the maximum at 374 nm, most likely due to the π - π^* transitions in less conjugated chains coming from the oligomeric fractions. To prove this, the UV-Vis absorption spectrum of PProDOT-OH was also registered in DCM, a solvent that can dissolve only oligomeric fractions of this polymer. As expected, the absorption band revealed a blue shift in DCM compared to NMP (maximum at 382 nm) and overlapped with the weak absorption obtained in NMP (Figure 5a).

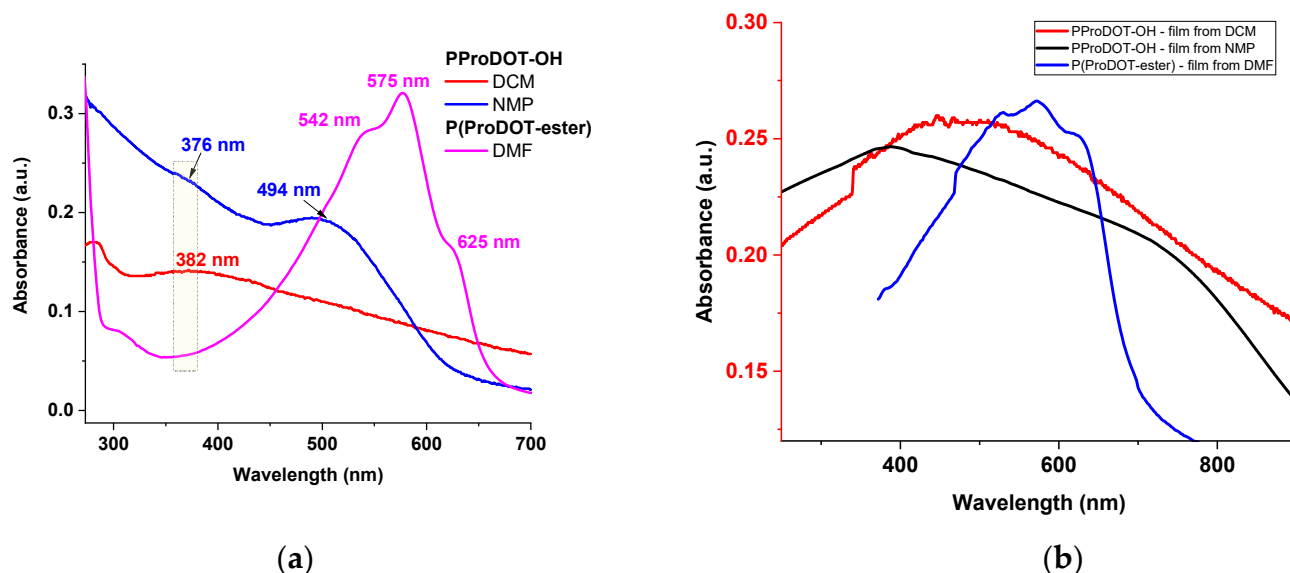


Figure 5. UV-vis absorption spectra of PProDOT-OH and P(ProDOT-ester) in solution (a) and solid state (b).

By further investigations of the photo-physical behavior in the solid state, no significant modifications were noticed between the solution and film absorptions for both polymers, except for an apparent broadening and small shifts (Figure 5b). Thus, the three maxima of P(ProDOT-ester) films were found at 528, 573, and 625 nm, while PProDOT-OH films

prepared from DCM and NMP showed an absorption band with one (470 nm) or two maxima (387 nm and 739 nm), respectively.

The fluorescence (FL) spectra of PProDOT-OH were initially measured in NMP solution by excitation at 380 nm and 500 nm (Figure 6a). By excitation at 380 nm, two emission bands were noticed in the FL spectrum, corresponding to the emission from both short and long polymer chains. Instead, by excitation at 500 nm, a dominant emission band was registered with a maximum at 611 nm that originated from the emission of long conjugated chains of PProDOT-OH. This perfectly overlapped with the lower energy band obtained by excitation at 380 nm, prompting us to consider that an excitation energy transfer from oligomeric fractions to the longer polymer chains occurred under 380 nm excitation. When P(ProDOT-ester) was excited at wavelengths corresponding to the main absorption maxima, a well-defined spectrum consisting of a single intense emission band with the main maximum at 610 nm was obtained (Figure 6a). The more extensive conjugation of PProDOT-ester did not lead to a bathochromic shift of the emission maximum with respect to that recorded for PProDOT-OH. On the other hand, the FL emission intensity was strongly influenced by the nature of the side substituent, with it being 102 times higher for PProDOT-OH compared to P(ProDOT-ester). In the solid-state, the studied ProDOT-based polymers displayed a quenched fluorescence, mostly due to the strong aggregation of the polymeric chains.

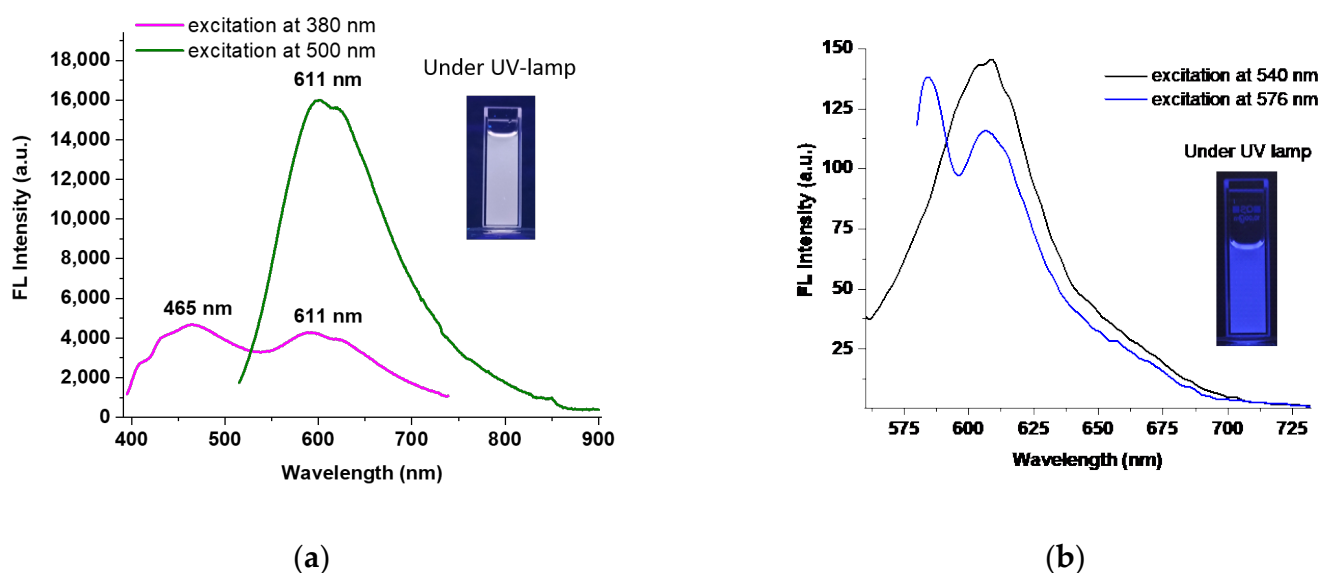


Figure 6. Fluorescence spectra of (a) PProDOT-OH and (b) P(ProDOT-ester) by excitation at different wavelengths.

3.3. Films Morphology

Since the morphology of the films coated on the ITO electrodes is expected to have a significant effect on the redox properties, and further on charge storage and electrochromic performance of the synthesized polymers, AFM measurements were employed. The coatings were prepared from DCM, as described in the Experimental Section 2. However, since PProDOT-OH film obtained from NMP had a different UV-vis absorption spectrum compared to that of the film prepared from DCM, the morphology of the first was also investigated. Figure 7 illustrates the topographic images obtained for the ProDOT-based polymer films. The root mean square roughness (RMS) values were about 45 nm and 24 nm for the PProDOT-OH films coated with NMP and DCM, respectively, while the morphology observed in AFM images was similar. Both films displayed grains of different dimensions dispersed on the surface that, in the case of NMP-coated film, are considerably higher, explaining the increased roughness of its surface. Instead, AFM characterization showed a different film morphology for P(ProDOT-ester) film. The surface was smooth

and homogeneous, with pores of different dimensions (diameters of micrometer sizes), which suggested the existence of a microporous morphology. According to these findings, we may conclude that the side chain substituent affects the solid-state packing of these ProDOT-based polymers, either by inducing strong molecular interactions, as in the case of CH₂OH functionality, or by creating voids due to less packed macromolecules, as noticed in the case of P(ProDOT-ester).

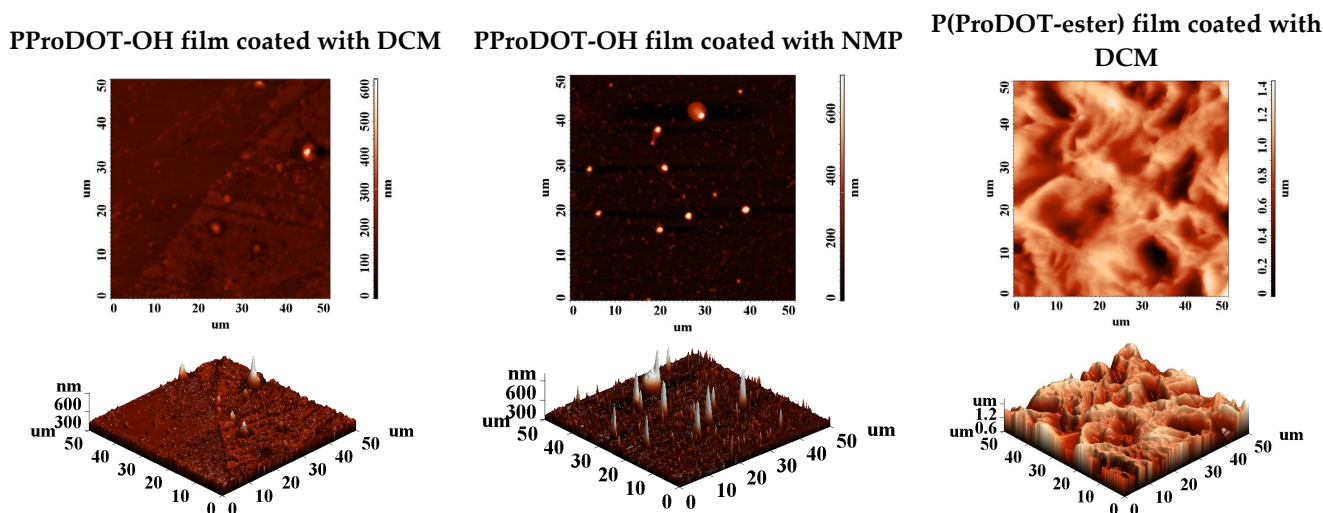


Figure 7. AFM images of ProDOT-based polymer films (scanned area 50 $\mu\text{m} \times 50 \mu\text{m}$, **top**: 2D image, **bottom**: 3D image).

3.4. Energy Storage Capability

The electrochemical characteristics of the synthesized ProDOT-based polymers were initially evaluated by cyclic voltammetry (CV) using a classical three-electrode electrochemical cell consisting of a thin polymer film drop-cast from DCM on the transparent indium tin oxide (ITO)-coated glass substrate as the working electrode, Pt wire as the counter electrode, and Ag/AgCl as the reference electrode. To assess the best conditions for electrochemical stability, and hence the electrical charge storage capability, P(ProDOT-ester) was first tested as electrode material in three organic electrolytes—lithium perchlorate (LiClO₄)/acetonitrile (ACN), tetrabutylammonium hexafluorophosphate (TBAF)/ACN, and tetrabutylammonium perchlorate (TBAP)/ACN. All CV curves were recorded at a scan rate of 50 mV/s, while the potential range was set between 0 and +1.3 V. The obtained CV curves are shown in Figure 8. By applying an electric potential, a color switch from purple to light green/blue occurred in all three cases, thus highlighting the electrochromic behavior of this polymer. While in LiClO₄/ACN, the oxidation peak of P(ProDOT-ester) was noticed at +0.53 V vs. Ag/AgCl, in the other two electrolyte systems, the oxidation occurred at higher potentials (+0.76 V vs. Ag/AgCl in TBAF/ACN and +0.75 V vs. Ag/AgCl in TBAP/ACN).

In all three cases, the oxidation is attributed to the electron release from the sulfur atom of the thiophene ring [28]. The anodic shift of the oxidation peak in different electrolytes is not surprising, considering the different capacities of ion transport across the polymer film interface. The stability of the polymer films over 10 repeated scans proved to be better in LiClO₄/ACN since no shift of the anodic peak nor decrease of the current intensity was observed in this electrolyte. Apart from this, the currents were considerably higher in LiClO₄/ACN system compared to the other two tested electrolyte systems.

In order to gain a deeper understanding of how charged states impact the conductivity of the of P(ProDOT-ester) coated on ITO electrode in the selected electrolyte systems, electrochemical impedance spectroscopy (EIS) was involved. This method allows measuring of the electrical response of the system in the frequency domain, which enables the sepa-

ration of resistive (real impedance) and capacitive or charge accumulation contributions (imaginary impedance). According to the Nyquist plots provided in Figure 9, obvious differences were found in terms of impedance response for these three systems. At high frequency, a distorted semicircle with different diameters was registered at 0 V due to the charge transfer process between the ITO/P(ProDOT-ester)/solution interfaces. In the medium to low-frequency region, a vertical line with different slopes was also recorded, being indicative of accumulation of ions at the electrode surface. The more vertical line obtained in TBAF/ACN and LiClO₄/ACN demonstrates a better capacitive behavior of the polymer in these systems compared to TBAP/ACN, without diffusion limitations. Furthermore, in TBAF/ACN and LiClO₄/ACN, the polymer displays lower semicircle diameter compared to TBAP/ACN, suggesting a better charge transfer activity between the polymer films and the solution interfaces, and hence polymer-coated electrodes of higher conductivity and capacitance. Thus, charge transfer resistance (R_{CT}) values of 0.84 k Ω /cm² (LiClO₄/ACN), 2.42 k Ω /cm² (TBAP/ACN), and 0.60 k Ω /cm² (TBAF/ACN) were obtained, being lower than those reported for related ProDOT-based polymers obtained by electropolymerization [10]. The greater the Ohm measurement of the charge transfer resistance, the greater the energy that is lost during the charge transfer. As a result, the interface between the P(ProDOT-ester) and TBAF/ACN and LiClO₄/ACN electrolytes demonstrates higher efficiency in terms of electrolyte ion diffusion and charge transfer, announcing better capacitive characteristics. However, considering the CV results and the low difference between the R_{CT} values obtained in these systems, LiClO₄/ACN electrolyte system was selected for subsequent capacitive studies.

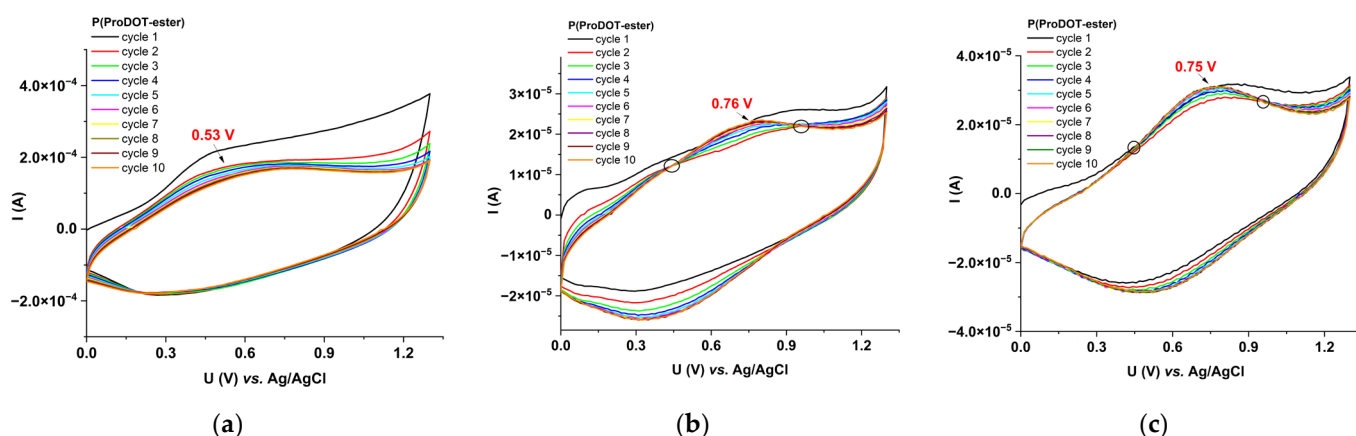


Figure 8. Cyclic voltammograms of ITO-coated P(ProDOT-ester) in different electrolyte systems, at 50 mV/s: (a) 0.1 M LiClO₄/ACN, (b) 0.1 M TBAF/ACN, and (c) 0.1 M TBAP/ACN.

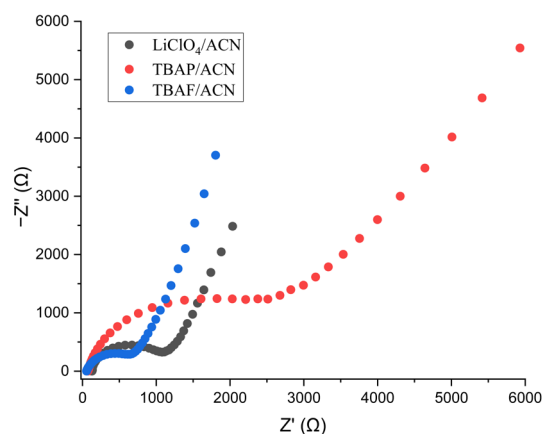


Figure 9. Nyquist spectra of P(ProDOT-ester) in various electrolytic systems.

Thus, to evaluate the electrical charge capacity of P(ProDOT-ester) as electrode material, the CV curves were performed in LiClO₄/ACN at different scan rates between 10 and 200 mV/s. The pattern of the curves was near rectangular, with small peaks (Figure 10a), indicating that the charge storage capability of this polymer is based on electro-oxidation and electro-reduction processes [21]. According to Figure 10, its electrochemical behavior is similar to those with a surface-confined coating due to the linear dependence of the redox peak currents by the scan rates specific for a diffusionless conducting polymer coating. At the end of positive potential window, the CVs displayed a fast current switching, suggesting the capacitor response of P(ProDOT-ester), similar to related polymers [29]. Usually, the CV pattern close to a rectangle is associated with a low resistance of the electrode material, whilst any distorted rectangular pattern with an oblique angle is an indication of an electrode material with high resistance [30]. The CV traces of P(ProDOT-ester)-based electrode display a distorted shape, indicating an ohmic resistance of the electron transfer and incomplete diffusion of electrolyte ions into the electrode surface [10].

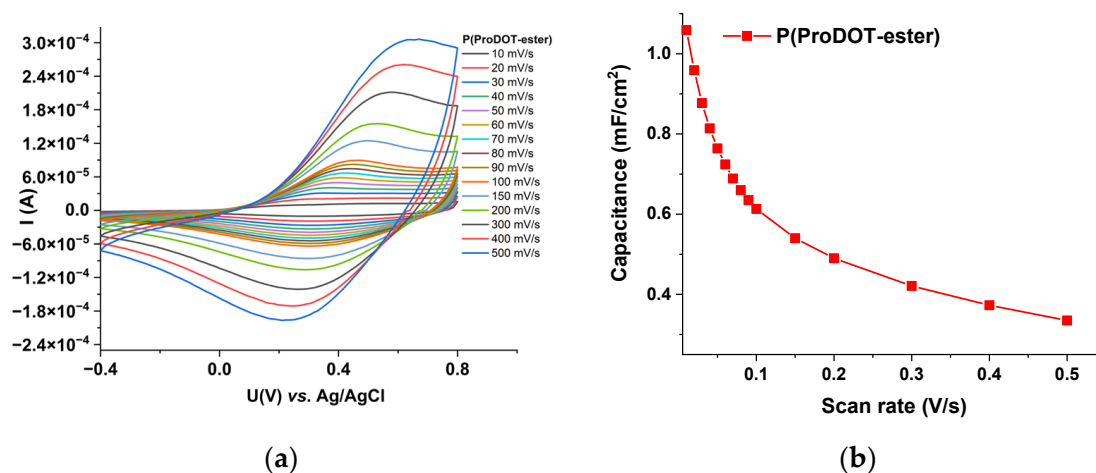


Figure 10. Cyclic voltammograms of P(ProDOT-ester) electrode at different scan rates (a) and evolution of the specific areal capacitance with the scan rate (b).

The specific areal capacitance estimated from the CV curves was calculated according to the following equation [10]:

$$C_{a,CV} = \frac{\int I(V)dV}{2vA\Delta V} \quad (1)$$

where $\int I(V)dV$ is the integrated area of the CV curve, v is the scan rate (V/s), A is the active area of the electrode surface (cm²), and ΔV is the potential window (V).

The specific areal capacitance estimated from the CV curves decreased with increasing the scan rate, with the maximum capacitance obtained at a scan rate of 10 mV/s of 1.059 mF/cm² (Figure 10b). This suggests a good energy storage capability of P(ProDOT-ester)-based electrode, well explained by the microporous structure of the film (as observed in AFM images) that allows the transport of the low size electrolyte ions throughout the electrode material.

These results prompted further studies by means of chronopotentiometry to explore the galvanostatic charge–discharge (GCD) capability of P(ProDOT-ester)-based electrode at different current densities. First, the charge–discharge process was studied at a single current density, 0.01 mA/cm², and different intervals of time, until full charging, and thereafter this procedure was applied at different current densities. The saturation charge voltage (V_{sc}), which is the voltage accumulated in the electrodes and beyond that no further charging may occur, was measured according to the previous reports [31–33]. When the

saturation potential is attained, the electrode begins the discharge process. The GCD plots were used to calculate the specific areal capacitance according to the equation [34]:

$$C_{a,GCD} = \frac{I \times \Delta t}{\Delta V \times A} \quad (2)$$

where I is the discharge current (A), Δt is the discharge time (s), ΔV is the operational potential (0 to V_{sc}), and A is the active area of the electrode surface (cm^2).

A maximum areal capacitance of 0.538 mF/cm^2 resulted at 0.01 mA/cm^2 and a Coulombic efficiency of 83.87%. Figure 11a illustrates the GCD curves registered for P(ProDOT-ester) in the saturation regime at different current densities, while Figure 11b shows the Coulombic efficiencies of this electrode material at different GCD current densities. Similar to the results extracted from CV curves, the specific areal capacitance gradually decreased as the current density increased. This aspect is attributed to the diffusion of electrolytic ions and migration into the active material at low current density [21].

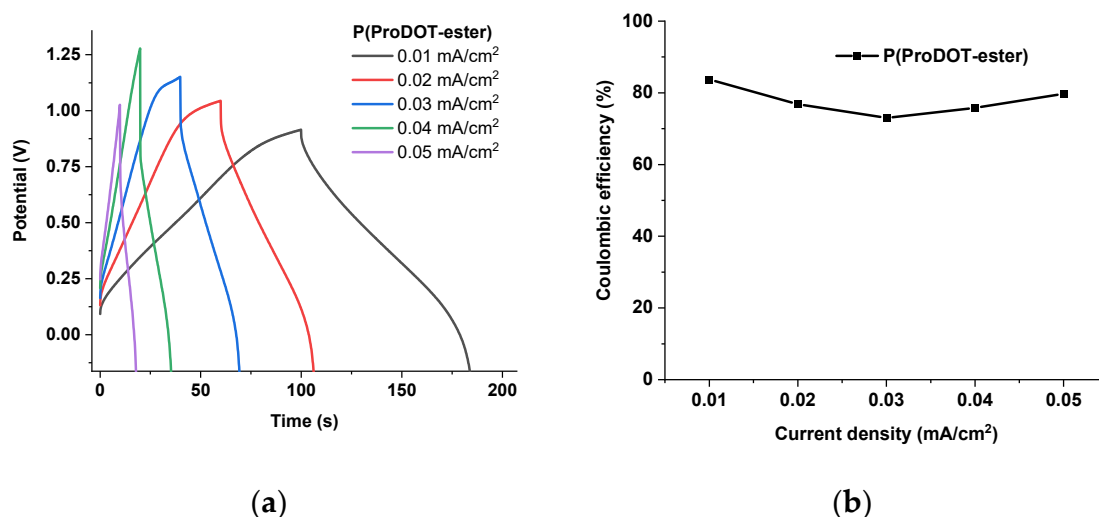


Figure 11. GCD plots (a) and Coulombic efficiencies (b) at different current densities of the P(ProDOT-ester) electrode material.

It should be noted that when fully charged, the P(ProDOT-ester) film changed its color from purple to light green/blue, while at discharge, it returned to its original color, demonstrating the suitability of this polymer for use in ESSWs applications.

Given the promising results obtained for P(ProDOT-ester), a similar protocol (0.1 M $\text{LiClO}_4/\text{ACN}$) was applied for the study of PProDOT-OH behavior as electrode material coated from DCM on ITO substrate. Although the CV curves were quite rectangular (Figure 12), unfortunately, no electrochromic behavior was observed for this polymer. This can be due to strong packed polymer chains in the solid state (as observed in AFM images), which impede an appropriate ion diffusion and charge transport throughout the entire electrode material. This can also explain the lower currents obtained for this polymer.

However, the CV curves for PProDOT-OH were also recorded at different scan rates between 10 and 500 mV/s (Figure 13a), and the specific areal capacitance was calculated accordingly. As expected, the capacitance dropped gradually with the increase of the scan rate, being approx. 1000 times lower (the order of μF) than the values obtained for P(ProDOT-ester) (Figure 13b). Thus, the maximum value of the specific areal capacitance was $3.32 \mu\text{F/cm}^2$ at 10 mV/s, indicating a weak electric charge storage capacity.

In order to achieve a better electric charge storage performance, a thick film was also drop-casted from DCM solution on ITO electrodes and investigated by CV at different scan rates. Although the maximum specific areal capacitance obtained from the CV curve at 10 mV/s was $11.81 \mu\text{F/cm}^2$, it also remained low (the order of μF). The GCD measure-

ments performed at different current densities, in the range of 0.001–0.003 mA/cm², led to the highest value of the specific areal capacitance of 4.65 μF/cm² at 0.001 mA/cm². These results provide support for the low capacity of PProDOT-OH to store charge due to the aggregated polymer chains in the solid state that led to a dense film morphology inappropriate for ions diffusion and transport.

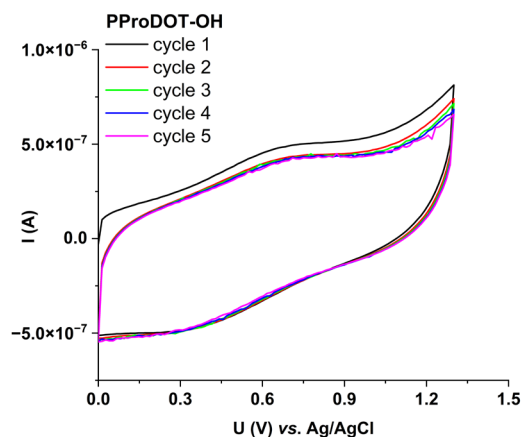


Figure 12. Cyclic voltammograms of PProDOT-OH on ITO substrate in 0.1 M LiClO₄/ACN at a scan rate of 50 mV/s.

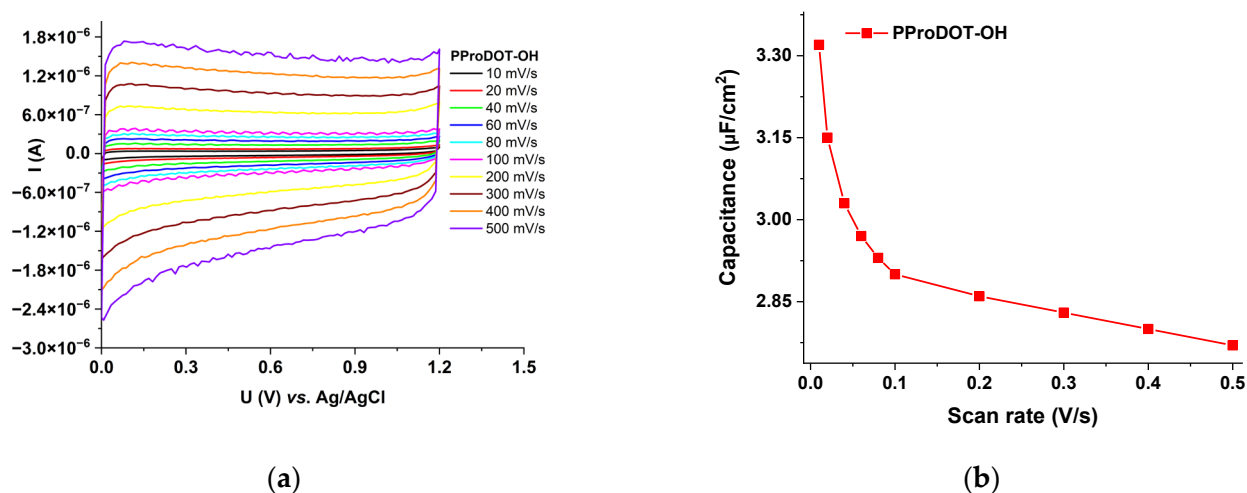


Figure 13. CVs of PProDOT-OH coated from DCM solution on ITO at different scan rates, in 0.1 M LiClO₄/ACN (a) and evolution of specific areal capacitance with the scan rate (b).

Considering that these modest results can also be attributed to the low solubility of PProDOT-OH in DCM, where practically only low molecular mass fractions can dissolve, another attempt was made to increase the capacitive behavior of this polymer by using as electrode material a thin polymer film prepared from NMP, a solvent that dissolves higher mass fractions of the polymer. In addition, the potential window was set from −0.4 V to +0.8 V to get more rectangular shaped CVs. But even in these conditions, the specific areal capacitance did not increase too much, with the maximum values being 27.93 μF/cm² at 10 mV/s and 11.11 μF/cm² at 0.001 mA/cm², as estimated from CV curves and GCD plots, respectively (Figure 14). These similar results to those obtained for the thick DCM films indicate that the conjugation length is less important to the polymer's capacity to store charge compared to the very dense, aggregated morphology of the film that induced a low-rate capability and also no electrochromic effect.

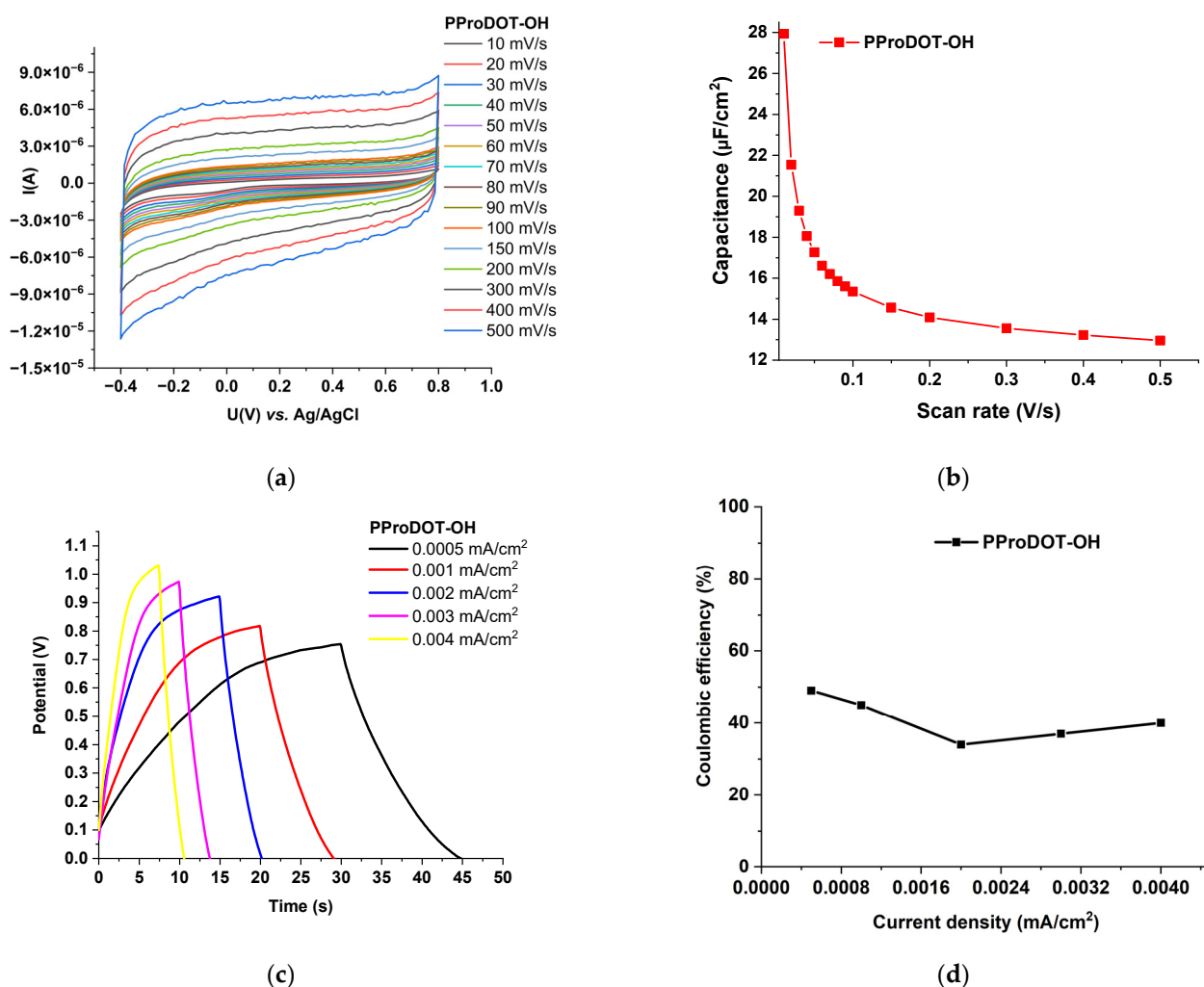


Figure 14. Electrochemical characteristics of PProDOT-OH film coated on ITO from NMP solution in 0.1 M LiClO₄/ACN: CVs at different scan rates (a); evolution of specific areal capacitance estimated from CVs with the scan rate (b); GCD plots at various current densities (c); Coulombic efficiencies at different GCD current densities (d).

3.5. Electrochromic Evaluation of P(ProDOT-Ester)

Since only P(ProDOT-ester) thin films deposited on ITO substrates changed color during CV and GCD experiments due to the oxidation of thiophene heterocycle, it was further investigated with regard to the electrochromic response and its stability over multiple switching steps. This involved monitoring the variation of the UV-vis absorption spectra during potential sweeps in a UV cuvette equipped with polymer-coated ITO as the working electrode, Pt wire as the auxiliary electrode, Ag wire as the reference electrode, and LiClO₄/ACN as the electrolyte. Figure 15 illustrates the spectral patterns of this polymer at different electrode potentials plotted as spectroelectrochemical curves.

In the neutral state, the polymer thin film showed the main absorption band with a maximum at 572 nm due to the π - π^* transitions from the conjugated polymer chains. By sweeping the potential with steps of 100 mV/s, some spectral changes occurred. Consequently, the main absorption band started to decrease very fast, while lower energy bands evolved in near infrared (NIR) at 941 nm. When the potential value was adjusted to 0.4 V, this NIR absorption band reversed its behaviour so that at 0.8 V, the polymer already reached the maximum oxidation process. After this, no important changes were observed in the UV-vis absorption spectra. As a result, the thin polymer film changed its

color from deep purple to highly transmissive green/blue. The transition between colored and transmissive states can also be viewed in the inset in Figure 15.

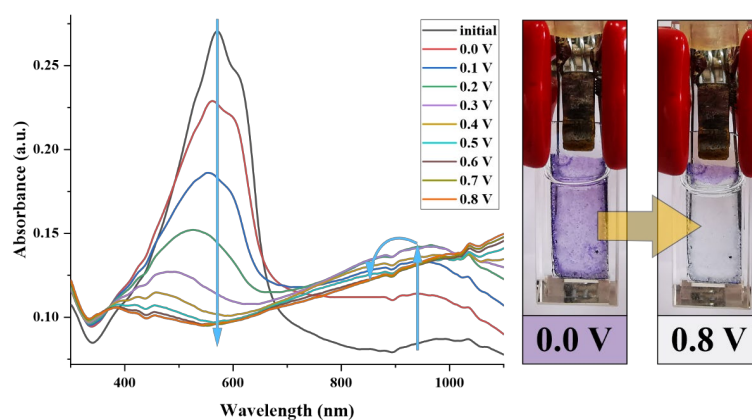


Figure 15. The electrochromic response of P(ProDOT-ester) thin film coated on ITO (coated area: $\sim 1.3 \text{ cm}^2$).

Going further, the electrochromic main parameters and stability of the synthesized polymer were investigated. To this aim, transmittance variation ($\Delta\%T$) as a function of time was assessed by setting the maximum potentials corresponding to the oxidation of the thiophene heterocycle and by monitoring the absorption bands at 572 nm. As a result, the response times were evaluated by applying repetitive square-wave potentials between -0.4 V (colored—neutral state) and 0.8 V (“bleached”—oxidized state), with a pulse width of 20 s. Based on 100 repeating cycles, the potential step absorptiometry curve of the P(ProDOT-ester) thin film was obtained, as shown in Figure 16.

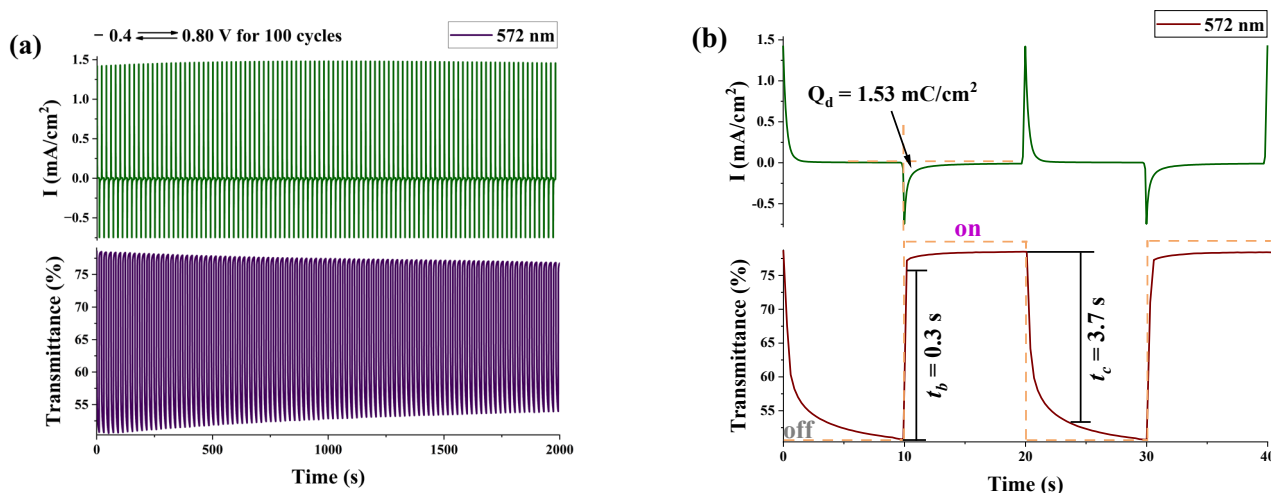


Figure 16. Potential step absorptiometry of ITO-coated P(ProDOT-ester) (coated area $\sim 1.3 \text{ cm}^2$): current and optical switching under potential sweep between -0.4 V and 0.8 V (100 cycles) with a pulse width of 20 s, monitored at $\lambda_{\text{max}} = 572 \text{ nm}$ (a); evaluation of the main parameters (b).

Hence, the polymer revealed an ultra-fast response towards “bleached” (oxidized state) of 0.3 s, and 3.7 s for coloring (neutral state). Moreover, the transmittance variation ($\Delta\%T$) was 27.7%. Based on these main parameters, the electrochromic coloration efficiency (CE, η) was calculated by employing the equation:

$$\eta = \Delta\text{OD}/Q_d \quad (3)$$

where ΔOD is the optical transmittance change ($\Delta OD = \log[T_{\text{bleached}}/T_{\text{colored}}]$) and Q_d (mC/cm^2) is the injected/ejected charge during a redox cycle. Accordingly, the P(ProDOT-ester) thin film showed a CE value of $123 \text{ cm}^2/\text{C}$. In addition, the long-term stability and reversibility of the electrochromic behaviour were investigated, and it was found that the studied ProDOT-based polymer exhibits a maximum CE decay of 9.9% after 100 cycles.

4. Conclusions

Two ProDOT-based polymers functionalized with CH_2OH or aromatic ester substituted -oligoether chains were prepared by oxidative chemical polymerization. After structural identification by FTIR and $^1\text{H-NMR}$ spectroscopy, the polymers were processed into thin coatings having either granular or microporous morphology, with dependence on the structural units of the side chains. The synthesized polymers were analyzed by UV-vis absorption and fluorescence spectroscopies, which evidenced the dependence of the absorption and emission maxima on the conjugation length of the polymers. When studied by cyclic voltammetry, only the ester functionalized polymer showed electrochromic behaviour, while the dense packed chains of the CH_2OH -substituted polymer completely suppressed this phenomenon through an inefficient ions diffusion and transport at the electrode surface. This is also the reason for the low capacitive behavior of this polymer that requires further processing strategies to prevent the hydrogen bonds development promoted by the OH groups. Instead, the ester-functionalized polymer demonstrated a high electrical storage capability, with the highest capacitance of $1.059 \text{ mF}/\text{cm}^2$ at a scan rate of $10 \text{ mV}/\text{s}$. In addition, this polymer switches its color from deep purple to highly transmissive green/blue when fully charged, while it returns to its original color at discharge, demonstrating its suitability for use in energy storage smart window applications.

Author Contributions: Conceptualization, M.-D.D. and A.-P.C.; methodology, M.-D.D., A.-P.C. and C.-P.C.; validation, M.-D.D., A.-P.C. and C.-P.C.; formal analysis, A.-P.C. and C.-P.C.; investigation, A.-P.C., C.-P.C. and M.-D.D.; resources M.-D.D.; data curation, M.-D.D.; writing—original draft preparation, A.-P.C., M.-D.D. and C.-P.C.; writing—review and editing, M.-D.D., A.-P.C. and C.-P.C.; supervision, M.-D.D.; project administration, M.-D.D.; funding acquisition, M.-D.D. All authors have read and agreed to the published version of the manuscript.

Funding: This work was supported by a grant of the Ministry of Research, Innovation and Digitization, CNCS-UEFISCDI, project number PN-III-P4-PCE-2021-1728 (contract number 46/2022) within PNCDI III.

Data Availability Statement: The data presented in this study are available on request from the corresponding author.

Conflicts of Interest: The authors declare no conflict of interest.

References

1. Groenendaal, L.; Zotti, G.; Aubert, P.; Waybright, S.M.; Reynolds, J.R. Electrochemistry of Poly(3,4-alkylenedioxythiophene) Derivatives. *Adv. Mater.* **2003**, *15*, 855–879. [[CrossRef](#)]
2. Lakshmanan, R.; Raja, P.P.; Shivaprakash, N.C.; Sindhu, S. Fabrication of fast switching electrochromic window based on poly(3,4-(2,2-dimethylpropylenedioxy)thiophene) thin film. *J. Mater. Sci. Mater. Electron.* **2016**, *27*, 6035–6042. [[CrossRef](#)]
3. Sikder, B.K. A step towards the processability of insoluble or partially soluble functional and structural variants of polymers based on 3,4-alkylenedioxythiophene. *RSC Adv.* **2016**, *6*, 107776–107784. [[CrossRef](#)]
4. Kausar, A. Overview on conducting polymer in energy storage and energy conversion system. *J. Macromol. Sci. Part A Pure Appl. Chem.* **2017**, *54*, 640–653. [[CrossRef](#)]
5. Raza, S.; Li, X.; Soyekwo, F.; Liao, D.; Xiang, Y.; Liu, C. A comprehensive overview of common conducting polymer-based nanocomposites; Recent advances in design and applications. *Eur. Polym. J.* **2021**, *160*, 110773. [[CrossRef](#)]
6. Namsheer, K.; Rout, C.S. Conducting polymers: A comprehensive review on recent advances in synthesis, properties and applications. *RSC Adv.* **2021**, *11*, 5659–5697.
7. Tran, V.V.; Lee, S.; Lee, D.; Le, T.H. Recent Developments and Implementations of Conductive Polymer-Based Flexible Devices in Sensing Applications. *Polymers* **2022**, *14*, 3730. [[CrossRef](#)]
8. Kaloni, T.P.; Giesbrecht, P.K.; Schreckenbach, G.; Freund, M.S. Polythiophene: From Fundamental Perspectives to Applications. *Chem. Mater.* **2017**, *29*, 10248–10283. [[CrossRef](#)]

9. Hebert, D.D.; Naley, M.A.; Cunningham, C.C.; Sharp, D.J.; Murphy, E.E.; Stanton, V.; Irvin, J.A. Enabling Conducting Polymer Applications: Methods for Achieving High Molecular Weight in Chemical Oxidative Polymerization in Alkyl- and Ether-Substituted Thiophenes. *Materials* **2021**, *14*, 6146. [[CrossRef](#)]
10. Karazehir, T.; Sarac, B.; Gilsing, H.D.; Eckert, J.; Sarac, A.S. Oligoether Ester-Functionalized ProDOT Copolymers on Si/Monolayer Graphene as Capacitive Thin Film Electrodes. *J. Electrochem. Soc.* **2020**, *167*, 070543. [[CrossRef](#)]
11. Guler, F.G.; Gilsing, H.D.; Schulz, B.; Sarac, A.S. Impedance and Morphology of Hydroxy- and Chloro-Functionalized Poly(3,4-propylenedioxythiophene) Nanostructures. *J. Nanosci. Nanotechnol.* **2012**, *12*, 7869–7878. [[CrossRef](#)]
12. Mishra, S.P.; Sahoo, R.; Ambade, A.V.; Contractor, A.Q.; Kumar, A. Synthesis and characterization of functionalized 3,4-propylenedioxythiophene and its derivatives. *J. Mater. Chem.* **2004**, *14*, 1896–1900. [[CrossRef](#)]
13. Wei, B.; Ouyang, L.; Liu, J.; Martin, D.C. Post-polymerization functionalization of poly(3,4-propylenedioxythiophene) (PProDOT) via thiol–ene “click” chemistry. *J. Mater. Chem. B* **2015**, *3*, 5028–5034. [[CrossRef](#)]
14. Damaceanu, M.D.; Gilsing, H.D.; Schulz, B.; Arvinte, A.; Bruma, M. An easily functionalizable oligo(oxyethylene)- and ester-substituted poly(3,4-propylenedioxythiophene) derivative exhibiting alkali metal ion response. *RSC Adv.* **2014**, *4*, 52467–52475. [[CrossRef](#)]
15. Argun, A.A.; Aubert, P.H.; Thompson, B.C.; Schwendeman, I.; Gaupp, C.L.; Hwang, J.; Pinto, N.J.; Tanner, D.B.; MacDiarmid, A.G.; Reynolds, J.R. Multicolored Electrochromism in Polymers: Structures and Devices. *Chem. Mater.* **2004**, *16*, 4401–4412. [[CrossRef](#)]
16. Christiansen, D.T.; Ohtani, S.; Chujo, Y.; Tomlinson, A.L.; Reynolds, J.R. All Donor Electrochromic Polymers Tunable across the Visible Spectrum via Random Copolymerization. *Chem. Mater.* **2019**, *31*, 6841–6849. [[CrossRef](#)]
17. Perera, K.; Yi, Z.; You, L.; Ke, Z.; Mei, J. Conjugated electrochromic polymers with amide-containing side chains enabling aqueous electrolyte compatibility. *Polym. Chem.* **2020**, *11*, 508–516. [[CrossRef](#)]
18. Savagian, L.R.; Österholm, A.M.; Ponder, J.F.; Barth, K.J.; Rivnay, J.; Reynolds, J.R. Balancing Charge Storage and Mobility in an Oligo(Ether) Functionalized Dioxythiophene Copolymer for Organic- and Aqueous-Based Electrochemical Devices and Transistors. *Adv. Mater.* **2018**, *30*, 1804647. [[CrossRef](#)]
19. Ma, X.; Zhou, W.; Mo, D.; Zhang, K.; Wang, Z.; Jiang, F.; Hu, D.; Dong, L.; Xu, J. Electrochemical preparation of poly(2,3-dihydrothieno[3,4-b][1,4]dioxin-2-yl)methanol)/carbon fiber core/shell structure composite and its high capacitance performance. *J. Electroanal. Chem.* **2015**, *743*, 53–59. [[CrossRef](#)]
20. Ersozoglul, M.G.; Gilsing, H.D.; Gencturk, A.; Sarac, A.S. A Novel Dioxythiophene Based Conducting Polymer as Electrode Material for Supercapacitor Application. *Int. J. Electrochem. Sci.* **2019**, *14*, 9504–9519. [[CrossRef](#)]
21. Niu, J.; Chen, S.; Zhang, W.; Zhang, W.; Chai, K.; Ye, G.; Li, D.; Zhou, W.; Duan, X.; Xu, J. Supercapacitor properties of nanowire poly((3,4-dihydro-2-H -thieno[3,4- b][1,4]dioxepin-3-yl)methanol) free-supporting films. *Electrochim. Acta* **2018**, *283*, 488–496. [[CrossRef](#)]
22. Sarac, A.S.; Gilsing, H.D.; Gencturk, A.; Schulz, B. Electrochemically polymerized 2,2-dimethyl-3,4-propylenedioxythiophene on carbon fiber for microsupercapacitor. *Prog. Org. Coat.* **2007**, *60*, 281–286. [[CrossRef](#)]
23. Kim, J.; Rémond, M.; Kim, D.; Jang, H.; Kim, E. Electrochromic Conjugated Polymers for Multifunctional Smart Windows with Integrative Functionalities. *Adv. Mater. Technol.* **2020**, *5*, 1900890. [[CrossRef](#)]
24. Tong, Z.; Tian, Y.; Zhang, H.; Li, X.; Ji, J.; Qu, H.; Li, N.; Zhao, J.; Li, Y. Recent advances in multifunctional electrochromic energy storage devices and photoelectrochromic devices. *Sci. China Chem.* **2017**, *60*, 13–37. [[CrossRef](#)]
25. Kros, A.; Nolte, R.J.M.; Sommerdijk, N.A.J.M. Poly(3,4-ethylenedioxythiophene)-Based Copolymers for Biosensor Applications. *J. Polym. Sci. Part A Polym. Chem.* **2002**, *40*, 738–747. [[CrossRef](#)]
26. Reeves, B.D.; Unur, E.; Ananthakrishnan, N.; Reynolds, J.R. Defunctionalization of Ester-Substituted Electrochromic Dioxythiophene Polymers. *Macromolecules* **2007**, *40*, 5344–5352. [[CrossRef](#)]
27. Shi, P.; Amb, C.M.; Dyer, A.L.; Reynolds, J.R. Fast Switching Water Processable Electrochromic Polymers. *ACS Appl. Mater. Interfaces* **2012**, *4*, 6512–6521. [[CrossRef](#)]
28. Grzes, G.; Wolski, K.; Uchacz, T.; Bała, J.; Louis, B.; Scheblykin, I.G.; Zapotoczny, S. Ladder-like Polymer Brushes Containing Conjugated Poly(Propylenedioxythiophene) Chains. *Int. J. Mol. Sci.* **2022**, *23*, 5886. [[CrossRef](#)]
29. Hsu, C.Y.; Chen, H.W.; Lee, K.M.; Hu, C.W.; Ho, K.C. A dye-sensitized photo-supercapacitor based on PProDOT-Et₂ thick films. *J. Power Source* **2010**, *195*, 6232–6238. [[CrossRef](#)]
30. Chen, Y.; Xu, J.H.; Mao, Y.W.; Yang, Y.J.; Yang, W.Y.; Li, S.B. Electrochemical performance of graphene-polyethylenedioxythiophene nanocomposites. *Mater. Sci. Eng. B-Adv.* **2013**, *178*, 1152–1157. [[CrossRef](#)]
31. Manjakkal, L.; Navaraj, W.T.; Núñez, C.G.; Dahiya, R. Graphene–graphite polyurethane composite based high-energy density flexible supercapacitors. *Adv. Sci.* **2019**, *6*, 1802251. [[CrossRef](#)]
32. Niaz, N.A.; Shakoor, A.; Imran, M.; Khalid, N.R.; Hussain, F.; Kanwal, H.; Maqsood, M.; Afzal, S. Enhanced electrochemical performance of MoS₂/PPy nanocomposite as electrodes material for supercapacitor applications. *J. Mater. Sci. Mater. Electron.* **2020**, *31*, 11336–11344. [[CrossRef](#)]

33. Butnaru, I.; Chiriac, A.P.; Constantin, C.P.; Damaceanu, M.D. Insights into MWCNTs/polyimide nanocomposites: From synthesis to application as free-standing flexible electrodes in low-cost micro-supercapacitors. *Mater. Today Chem.* **2022**, *23*, 100671. [[CrossRef](#)]
34. Ni, D.; Chen, Y.; Song, H.; Liu, C.; Yang, X.; Cai, K. Free-standing and highly conductive PEDOT nanowire films for high-performance all-solid-state supercapacitors. *J. Mater. Chem. A* **2019**, *7*, 1323–1333. [[CrossRef](#)]

Disclaimer/Publisher's Note: The statements, opinions and data contained in all publications are solely those of the individual author(s) and contributor(s) and not of MDPI and/or the editor(s). MDPI and/or the editor(s) disclaim responsibility for any injury to people or property resulting from any ideas, methods, instructions or products referred to in the content.